JOURNAL OF MATERIALS SCIENCE 2 (1967) 78–87

An Oxidation Study of Ni-Cr-Fe Alloys in Carbon Dioxide at 800 to 1000° C

J. M. FRANCIS, J. A. JUTSON, J. H. BUDDERY
Materials Division, Central Electricity Generating Board, Berkeley Nuclear Laboratories, Berkeley, Glos, UK

Received 22 August 1966

Nickel-based alloys containing chromium and iron are alternative high-temperature materials to austenitic stainless steels at temperatures in excess of 800° C in gas-cooled reactor systems. In particular, some of the commercial superalloys may find application as cladding for ceramic fuel elements. These complex alloys contain a number of minor constituents that appear to play an ill-defined but essential role in regulating mechanical properties and oxidation resistance.

This paper describes a structural evaluation of thin, oxide films formed on two such alloys, Hastelloy X and Inconel 600, under representative reactor conditions, with emphasis on the application of electron and X-ray diffraction techniques for the identification of multicomponent, surface oxide phases. The difficulties and limitations of these techniques in relation to the complexity of the oxide under examination are apparent, but nevertheless the large amount of useful information obtained has enabled some understanding of the oxidation mechanism. As in the case of highly alloyed, chromium-nickel steels, the rate-determining step in the growth of surface oxide on both alloys appears to be cation diffusion through an initially formed, chromic oxide phase, resulting in the subsequent development of an outer spinel oxide of variable composition.

1. Introduction

The advent of a Civil Advanced Gas-Cooled Reactor (AGR) has produced demands for a high-temperature, fuel-cladding alloy with better oxidation resistance than the existing 20%Cr/25%Ni/Nb-stabilised steel, and the commercial nickel-base alloys have been suggested for this purpose for operating temperatures above 800° C.

These "superalloys" have inherently good oxidation resistance from the standpoint of general attack, although they have obvious disadvantages in terms of neutron absorption and ease of fabrication. The long-term oxidation resistance of several of these alloys has been investigated in air [1], when it was found that Hastelloy X had a greater resistance to oxidation than other similar alloys. Hastelloy X is currently considered to be the most suitable of the available alloys for evaluation in an AGR system.

In the present study, the structures of thin oxide films formed on Hastelloy X in pure carbon dioxide are compared with those formed on Inconel 600, which is another of the more important alloys in this series. No attempt has been made to supplement the rapidly accumulating kinetic data for these alloys in carbon dioxide-based atmospheres, but information relating to the surface oxide phases has been obtained by electron microscopy, electron and X-ray diffraction methods.

2. Materials

The actual compositions of the alloys studied, together with their nominal compositions are listed in table I. Specimens (2.0 × 1.5 × 0.03 cm) were sheared from cold-rolled strip, vacuum annealed at 1000° C for 2 h, and electropolished in a 10% solution of sulphuric acid in ethanol at 4 V and 0.3 A/cm².

TABLE I Composition of nickel-base alloys.

Alloy		Wt %										
		Ni	Cr	Mo	Fe	Co	C	Si	Mn	Ti	Al	W
Hastelloy X	Analysis	47.6	21.0	8.9	18.8	1.8	0.08	0.8	0.47	—	—	0.5
	Nominal composition	Bal	20.5 to 23.0	8.0 to 10.0	17.0 to 20.0	0.5 to 2.5	0.05 to 0.15	⩽1.0	⩽1.0	—	—	0.2 to 1.0
Inconel 600	Analysis	76.5	15.0	—	7.4	—	0.03	0.18	0.10	0.22	0.5	—
	Nominal	Bal	15.0	—	7.0	—	0.04	0.20	⩽1.0	0.3	⩽1.0	—

Reactor-grade carbon dioxide was purified by passing the gas through a column of finely divided copper at 300° C to remove oxygen, followed by a bed of magnesium perchlorate to remove moisture. The residual impurities consisted of less than 2 vpm* of oxygen and 3 vpm of water [2].

3. Structure of the Alloys

Both alloys are basically in the fcc γ-phase field of the Fe-Cr-Ni ternary phase diagram [3], but their mechanical properties are largely determined by the matrix distribution of intermetallic phases, such as $Ni_3(Ti, Al)$ in Inconel, and/or carbide phases of the structure type $M_{23}C_6$ or M_6C in Hastelloy. The metal portion of the carbide phase usually consists of chromium, molybdenum and/or tungsten.

The presence of increased amounts of molybdenum and tungsten in Hastelloy favours the formation of the more stable M_6C carbide, which does not dissolve at operational temperatures and thus restricts grain growth. Brunhouse and Titus [4] have identified M_6C carbide particles in Hastelloy with lattice parameters in the range 10.88 to 11.00 Å. An increasing nickel content was found to decrease the lattice parameter of the phase, whereas an increasing molybdenum content increased it.

4. Oxidation and Examination

After weighing and measuring, the strip specimens were placed in a silica boat at the centre of a silica tube, positioned inside a horizontal electric furnace. The reaction tube was evacuated and the furnace raised to temperature, after which carbon dioxide was admitted to the apparatus. A flow rate of ~50 cm³/min was maintained over the specimens throughout the oxidation periods. At the end of each oxidation, the reaction tube was again evacuated, and the specimens allowed to cool slowly over a 6 to 8 h period before removal from the apparatus.

The outer oxide surface of each specimen was directly examined in a Trüb-Täuber KD3m diffractograph using a 50 kV electron beam at grazing incidence. The oxide films were then chemically stripped from the underlying alloy using the standard iodine-methanol dissolution technique [5], and Debye-Scherrer patterns were obtained from the powdered oxide in each case using primary CuKα radiation.

5. Results

5.1. Weight Gain/Time Data

Previous experience with other systems has shown that the structure of the initially formed, surface oxide film can largely determine the subsequent growth of the various oxide phases formed on a complex high-temperature alloy. For this reason, a logarithmic scale of oxidation times was selected to enable examination of the surface film after successive exposure times of 0.1, 1, 10, and 100 h, and the weight-gain results are therefore plotted logarithmically.

At 800 and 900° C, the oxide film formed on Inconel was found to be partially non-adherent, so that areas from which the oxide had spalled could be detected on some specimens after cooling from the reaction temperature. The weight-gain data refer to adherent oxide as no provision was made for the collection of spalled oxide either during the exposure period or during the final cooling of each specimen. Consequently

*Volume parts per million

there are discontinuities in the data for Inconel at 800 and 900° C.

To aid comparison with the thermogravimetric data obtained at other laboratories, the weight gains for individual specimens of each alloy are plotted in figs. 1 and 2. Considerable care should be exercised in the interpretation of these curves in terms of the established growth-laws. Theoretical, linear, parabolic, and cubic oxidation rates have been inserted where appropriate to assist in this type of interpretation.

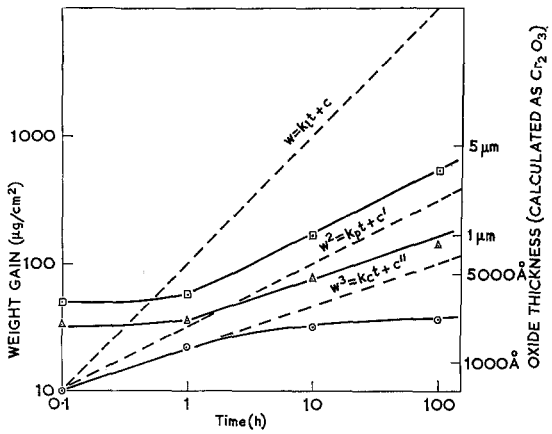

Figure 1 Weight gain/time curves for Hastelloy X; ○ – 800° C, △ – 900° C, □ – 1000° C.

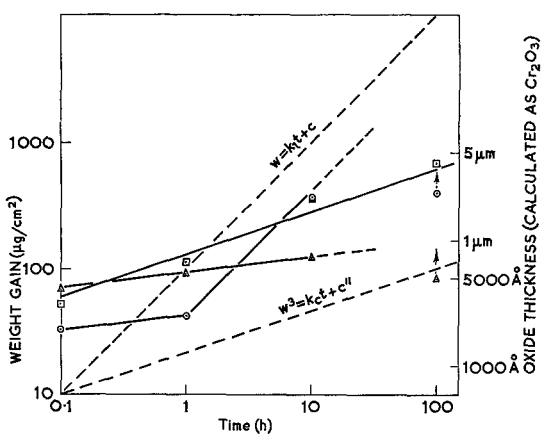

Figure 2 Weight gain/time curves for Inconel 600; ○ – 800° C, △ – 900° C, □ – 1000° C.

5.2. Electron Diffraction

The technique of reflection electron diffraction is limited to identification of specific phase types in the outer 20 to 50 Å of a smooth, surface oxide film, or in surface projections less than 1000 Å thick in the beam direction. In the present investigation, these consisted of (i) a rhombohedral (R) phase corresponding to either Cr_2O_3 or α-Fe_2O_3, or a solid solution of both, and (ii) a mixed oxide phase of the spinel (S) type, $M^{II}(M^{III})_2O_4$ or $M^{III}(M^{II}, M^{III})O_4$. In addition, other components present in the surface film such as M_6C carbide particles incorporated from the base alloy during growth of the film were sometimes detected. Because of the poor accuracy of lattice-parameter determination by this technique, individual members of a particular phase type cannot be resolved. The diffraction data obtained for both alloys are presented in table II; in every case, phase identification was based on at least six major reflections with an established accuracy of ± 0.05 Å.

5.3. X-ray Diffraction

The individual phases detected by X-ray diffraction analysis of the total oxide film, which was chemically stripped from the surface of each alloy, consisted of:

(*a*) A rhombohedral solid-solution phase of α-Fe_2O_3 and/or α-Al_2O_3 in Cr_2O_3, usually close to Cr_2O_3 in composition.

(*b*) A non-stoichiometric, spinel oxide phase in the lattice parameter range specifically described by Francis [6]: HPS – spinel phase, $Mn(Fe, Cr)_2O_4$; lattice parameter between 8.460 and 8.428 Å (range due to partial substitution of Fe and/or Cr); LPS – spinel phase; lattice parameter between 8.403 and 8.376 Å, contains Fe and Cr, or Ni not to exceed 0.45 mole fraction of $NiFe_2O_4$; LPS′ – spinel phase; lattice parameter between 8.376 and 8.341 Å, contains Fe and Ni, and may contain Cr; LPS″ – spinel phase; lattice parameter between 8.341 and 8.307 Å, contains both Ni and Cr.

(*c*) A cubic NiO phase.

(*d*) A metal carbide phase of the M_6C type.

Evaluation of the composition of these respective phases has been made on the basis of accurate, lattice-parameter determinations. Table III shows simply the qualitative proportions of each phase present as determined by visual estimation of line intensities. Figs. 3 to 5 show plots of the variation in lattice parameter of the spinel and rhombohedral phases. For comparison purposes, bands and lines corresponding to solid-solution phases and pure components are included in the graphs. Fig. 4 is a diagrammatic representation of the comparatively wide range of spinel oxides which may be encountered on Ni-Cr-Fe alloys, and may be compared directly

TABLE II Reflection electron diffraction data from surface oxide films formed on nickel-base alloys in carbon dioxide (code letters as defined in text and below table).

Exposure	800° C		900° C		1000° C	
(h)	Hastelloy X	Inconel 600	Hastelloy X	Inconel 600	Hastelloy X	Inconel 600
0.1	R S tr	R S tr	R S	R S	R S M_6C	R S tr
1	R S tr	R S tr	R S	R S	S	R S tr
10	R S M_6C tr	R S	R S M_6C	R S tr	R S M_6C tr	R S
100	S	R S	R S M_6C tr	R S tr	R	R S

tr - trace quantity only

TABLE III X-ray diffraction data from surface oxide films formed on nickel-base alloys in carbon dioxide (code letters as defined in text and below table).

Exposure	800° C		900° C		1000° C	
(h)	Hastelloy X	Inconel 600	Hastelloy X	Inconel 600	Hastelloy X	Inconel 600
0.1	R M_6C s w	R LPS′ NiO m s vw	R LPS M_6C s m w	R LPS′ NiO m m vw	R HPS M_6C m w m	R LPS′ NiO s w vvw
1	R M_6C s w	R LPS′ NiO m s vw	R LPS′ M_6C m m vw	R LPS′ NiO m m vw	R LPS M_6C m w m	R LPS′ NiO s w vvw
10	R HPS M_6C m m vw	R LPS′ NiO w m vvw	R HPS M_6C m s w	R LPS′ NiO m w vvw	R LPS M_6C m w m	R LPS s vw
100	R HPS M_6C s m vw	R LPS′ NiO w s vvw	R HPS M_6C s m w	R LPS s vw	R HPS M_6C m m vw	R s

s, m, w, vw – strong, medium, weak, very weak, respectively

with the lattice parameter variations plotted in fig. 3.

Using this approach to a study of the high-temperature oxidation of complex alloys, X-ray diffraction results indicate the relative amounts of each phase averaged over the total volume of the surface film, but give no information relating to the geometry of phase distribution. For this, the investigation relies heavily upon electron and optical microscopy, as described in the next section.

5.4. Metallography

After oxidation, the two alloys showed a marked difference in appearance under the optical microscope. Hastelloy showed preferential attack at grain boundaries after the shorter exposures (fig. 6), but thereafter formed a uniform, featureless film. Only after 100 h at 1000° C, when very small flakes of oxide spalled, most probably on cooling, to expose effectively the underlying alloy, was there any apparent variation in surface texture.

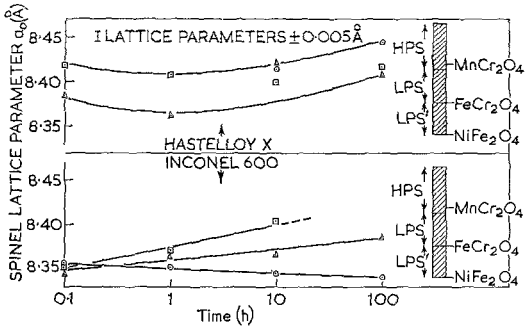

Figure 3 Lattice-parameter variations for spinel phases formed on both alloys; ○ – 800° C, △ – 900° C, □ – 1000° C.

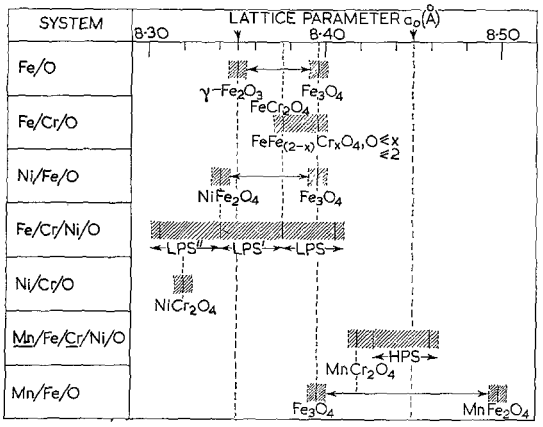

Figure 4 Systematic classification of spinel phases according to lattice parameter.

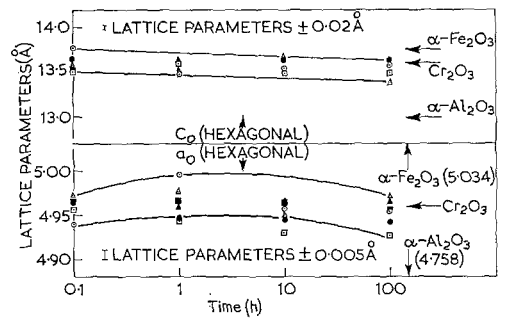

Figure 5 Lattice-parameter variations for rhombohedral oxide phases. Hastelloy X: ○ – 800° C, △ – 900° C, □ – 1000° C; Inconel 600: ● – 800° C, ▲ – 900° C, ■ – 1000° C.

Electron microscopy of stripped, oxide films removed from Hastelloy proved relatively unrewarding, since even after short exposures the oxide was sufficiently thick (> 1000 Å) to be generally opaque to an electron beam. Typical

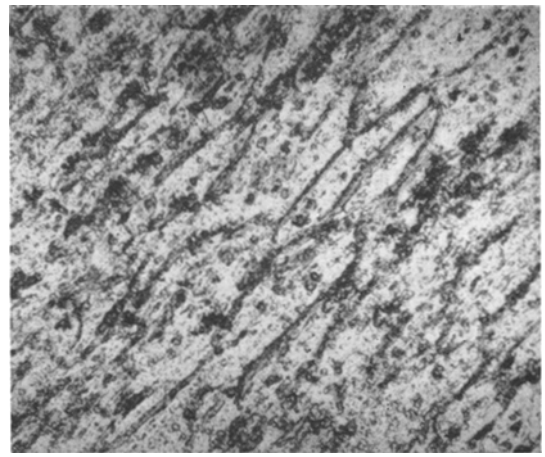

Figure 6 Grain-boundary attack on Hastelloy X after 0.1 h at 800° C (×125).

micrographs of occasional, thin areas (fig. 7) showed that the oxide at some boundaries was much thicker than that over the rest of the grains, and that the particle size was less than ~300 Å. A comparison of figs. 6 and 7 indicates that, whereas the grain size from fig. 6 was of the order of 50 μm, the "grain" size from fig. 7 was of the order of 5 to 10 μm. Clearly, the two micrographs cannot refer to the same features, and so the dark areas in fig. 7 must be coincident with some type of "subgrain" structure in the underlying alloy, possibly that associated with the matrix carbide distribution.

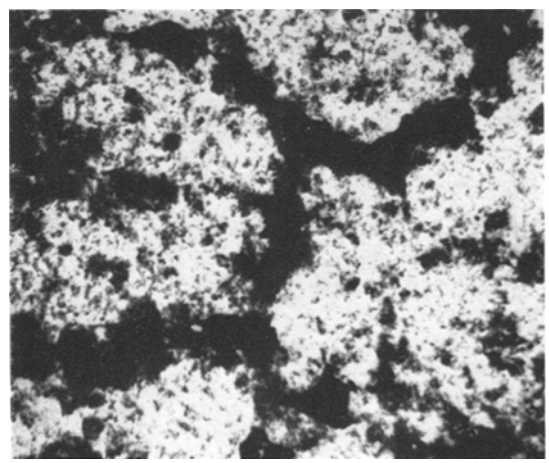

Figure 7 Transmission electron micrograph of stripped, oxide film from Hastelloy X after 0.1 h at 900° C (×5900).

In contrast to Hastelloy, oxidised specimens of Inconel showed a range of interesting features under the optical microscope. In the early stages of oxidation, there was attack at the centres of all the grains and much less at the grain boundaries (fig. 8), and, as oxidation continued, some grains (one in five) were clearly more severely attacked than others (fig. 9). At the longest exposure times, examination of the surface afforded little useful information, apart from the fact that at the higher temperatures the surface oxide appeared fairly thick and uniform, suggesting that the plasticity of the oxide had increased, thus considerably reducing the percentage of spalled oxide.

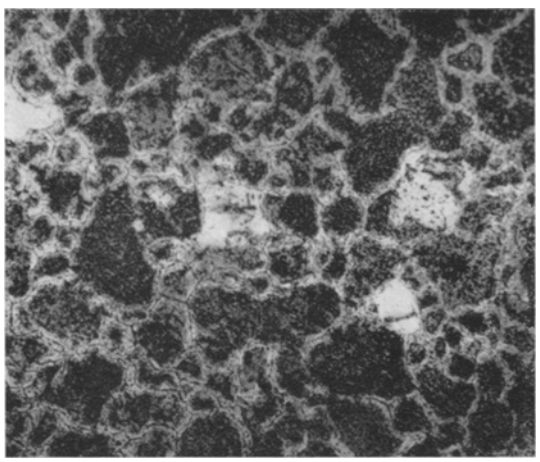

Figure 8 Localised attack on Inconel 600 after 1 h at 800° C (×100).

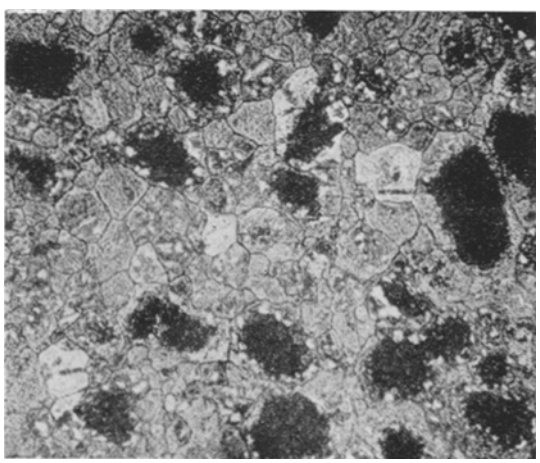

Figure 9 Attack at the centres of large grains on Inconel 600 after 1 h at 900° C (×125).

Microscopic examination of polished cross-sections of Inconel oxidised at 800° C showed localised areas of metal (presumably nickel) lying parallel to the alloy/oxide interface, embedded in the oxide. Regions of internal oxidation in the matrix alloy corresponded with the appearance of free metal in the surface film. At 1000° C, there was in addition slight, intergranular attack. The oxide layer consisted of two regions, a featureless but fairly uniform, outer layer (~3 μm thick) and a discontinuous, inner layer (~1 μm thick) of a granular nature (fig. 10).

6. Discussion

6.1. General Features of Oxidation Behaviour

A number of techniques have been used to obtain information on the structure and composition of the surface oxide phases formed on two N-Cr-Fe alloys, Hastelloy X, and Inconel 600. The information collected can best be interpreted in terms of the schematic oxidation behaviour shown in fig. 11.

In outline, the oxidation behaviour of Hastelloy appeared to follow the same course at each temperature. Even after the shortest oxidation periods, the oxide structure consisted of a rhombohedral phase overlaid by an uneven, spinel layer. These two phases continued to develop at the same rate so that roughly equivalent amounts of each phase were present over the whole exposure range. At the highest temperature, there was some evidence for grain boundary and surface diffusion of the rhombohedral phase resulting in appreciable coverage of the surface by this phase. M_6C carbide precipitates were incorporated unchanged into the growing oxide film.

In contrast to Hastelloy, the behaviour of Inconel after long oxidation times showed a considerable difference at 800 and 1000° C. In the fairly early stages of oxidation (up to 1 μm oxide thickness), the oxide structure consisted of two layers – a rhombohedral layer containing some NiO particles overlaid by a spinel layer. After long periods at 800° C, the thickness of the rhombohedral layer decreased and the NiO particles disappeared. The spinel layer, however, increased in thickness presumably as a result of the reaction $NiO + Cr_2O_3 \rightarrow NiCr_2O_4$. In contrast, at 1000° C, the spinel layer did not increase in thickness, but a much thicker, rhombohedral layer was formed under-

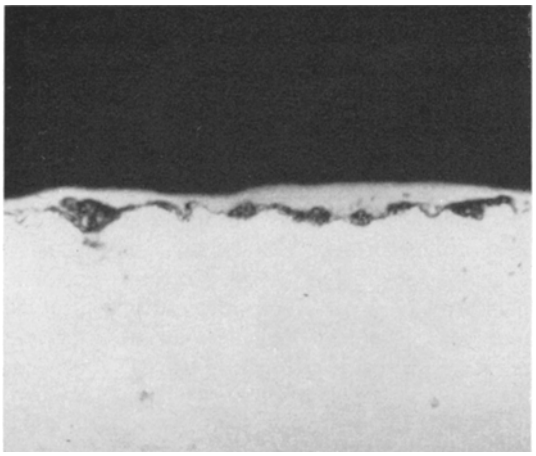

Figure 10 Cross-section of surface oxide formed on Inconel 600 after 100 h at 1000° C (×1000).

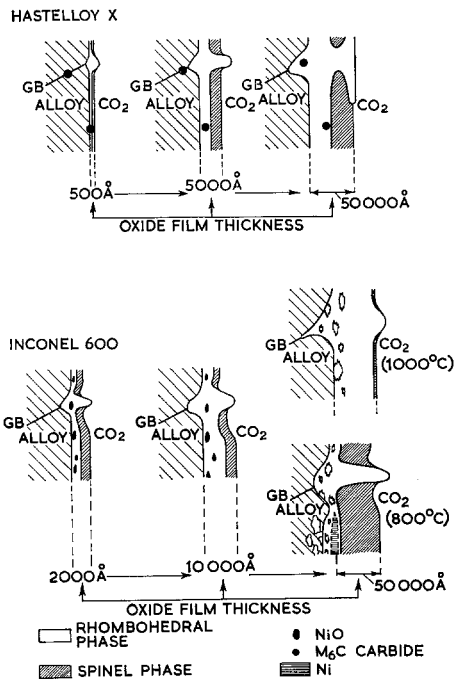

Figure 11 Schematic oxidation behaviour of Hastelloy X and Inconel 600.

neath. In both cases, an apparently porous, oxide layer was formed beneath the compact, outer layers. At low temperatures, some internal oxidation of the matrix alloy occurred with concurrent appearance of unreacted, metallic nickel dispersed in the porous, inner, oxide layer. More detailed reasons for various aspects of the oxidation behaviour illustrated in fig. 11 are discussed in the following sections.

6.2. Kinetic Data

It has already been pointed out that the research described here was designed for the study of oxide structure and not reaction kinetics. The kinetic data are consequently sparse. A direct comparison between Hastelloy and Inconel on the basis of figs. 1 and 2 shows that Hastelloy behaves extraordinarily well (for exposure times up to 100 h) at 800° C with a rate law even slower than cubic, very well at 900° C with an approximately cubic rate law, and quite well at 1000° C with a parabolic rate law. Inconel, however, behaves relatively poorly at 800° C owing to spalling of a brittle, surface oxide, rather better at 900° C again with some spalling, and at 1000° C the kinetics seem even more favourable than Hastelloy X at this temperature, in that the weight gains are smaller, the rate law is more nearly cubic and there is no evidence of spalling.

6.3. Composition of Oxide Phases as Deduced from X-ray Measurements

6.3.1. Spinel Phase

Previous work [6, 7] has shown some of the relationships that exist between the compositions and lattice parameters of spinel phases formed on Fe-Cr-Ni-Mn alloys. (Fig. 4 is reproduced from reference 6.) It is not possible unambiguously to ascribe a specific composition to a measured, lattice parameter, but Ni^{2+} and Cr^{3+} lower the lattice parameter whereas Mn^{2+} and Fe^{3+} increase it; the extreme end of the lattice-parameter scale corresponding to $NiCr_2O_4$ and $MnFe_2O_4$*.

The composition of the oxide initially formed on an alloy is determined by the free energy of formation of the various oxides, and the availability of the relevant elements at the alloy/oxide interface. From fig. 12, free-energy considerations favour oxidation in the order Mn > Cr > Fe > Ni. The availability of metal favours oxidation in the order Ni > Cr > Fe > Mn for the initially formed oxide, but, once this has formed and caused surface depletion of a particular element, then the subsequent oxide composition is also determined by the relative rate of diffusion of this element from the bulk of the alloy. From free-energy and availability considerations, the formation of chromium oxide would appear to be most favoured. Examination of the experimental data in the light of the above comments enables the following conclusions to be drawn.

*Inconel also contains ~0.5% Al. The effects of this on spinel composition are discussed later (section 6.4).

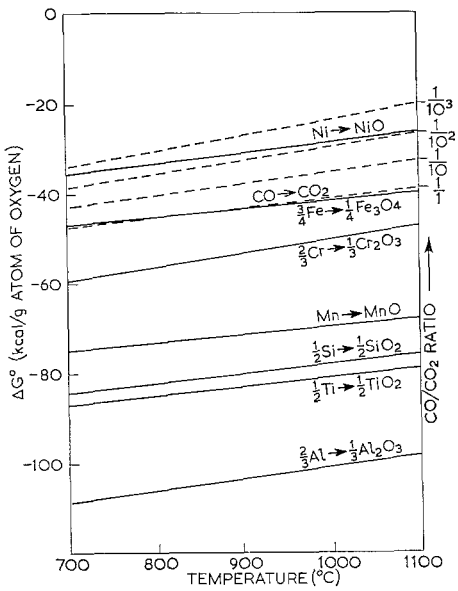

Figure 12 Standard free-energy diagram for the formation of metal oxides. Dotted lines refer to equilibrium gas mixtures of CO in CO_2.

On Inconel at 800° C, the spinel lattice parameter slowly fell towards the nickel-rich end of the range: this is consistent with the relatively low diffusion rates in the alloy at this temperature causing oxidation rates to be determined by the availability of nickel.

At 1000° C, on the other hand, the lattice parameter increased toward that corresponding to $MnCr_2O_4$ and is consistent with the much higher diffusion rates at this temperature, allowing diffusion of manganese from the bulk alloy and its selective oxidation at the surface. For long exposure times at the high temperature, the relative amount of spinel phase formed was very small: this is consistent with exhaustion of manganese in the thin sheet used. The 900° C data for Inconel fell mid-way between these two extremes, but are largely consistent with the higher temperature from the point of view of oxide structure.

On Hastelloy, which has a higher iron and manganese content than Inconel, the lattice parameter/temperature/time relationships might be expected to be more complex in view of the greater probability for the formation of iron-containing spinels. It is clear from fig. 3 that this is so, but at 1000° C there was a marked tendency for the composition of the spinel phase to approximate closely to $MnCr_2O_4$ at all exposure times. This reflects the greater availability of manganese in the base alloy.

6.3.2. Rhombohedral Phase

The rhombohedral oxide phase on these alloys can be formed from a solid solution within the range α-Fe_2O_3 through Cr_2O_3 to α-Al_2O_3. The same considerations of availability and thermodynamics mentioned before govern the composition of this phase, and this is borne out for Inconel by the lattice-parameter data (fig. 5). All the lattice parameters were exceedingly close to that of Cr_2O_3: only in the 800° C oxidation were the lattice parameters significantly lower, and if the lowering were due to the presence of α-Al_2O_3 then the α-Al_2O_3 content would not be greater than 10 wt % in the extreme case.

The data for Hastelloy are slightly less consistent, but the general conclusion is that there was no real evidence for the rhombohedral phase departing significantly from Cr_2O_3 in composition.

6.4. Significance of Minor Elements

The significance of manganese as a minor alloying element in both Hastelloy (0.5%) and Inconel (0.1%) has already been discussed with regard to spinel composition. In addition to manganese, Hastelloy contains silicon, and Inconel contains silicon, titanium, and aluminium. Owing to the high free-energy of formation of the corresponding oxides in carbon dioxide-based atmospheres (fig. 12), these elements may play an important role in determining the nature of the overall oxidation process.

Aluminium in particular can go into solid solution either in the rhombohedral or the spinel phase. It drastically lowers the lattice parameters of all these phases; the values for the pure phases are: $NiAl_2O_4$, $a = 8.048$ Å; $FeAl_2O_4$, $a = 8.113$ Å; $MnAl_2O_4$, $a = 8.258$ Å; α-Al_2O_3, $a = 4.758$ Å and $c = 12.991$ Å. Comparison of these figures with the observed parameters suggests that only small quantities of aluminium could be incorporated into the spinels and rhombohedral phases detected. However, the presence of aluminium and not nickel could be the reason why the lattice parameters of spinels formed on Inconel tend to be slightly lower than those formed on Hastelloy.

Silicon could be present as amorphous SiO_2 [8], in which case it could not have been detected by any of the experimental methods, or as a crystalline silicate. No evidence for the presence

of such a silicate was obtained. Titanium would seem most likely to be present either as TiO_2 or $M^{II}TiO_3$.

Although no evidence was obtained for the presence of minor elements other than manganese in the oxides formed on both alloys, this does not preclude their presence as very thin but possibly rate-determining films.

With Hastelloy, substantial amounts of molybdenum, cobalt, and tungsten are also present in the alloy. The evidence of previous workers [9] suggests that these elements play no important part in the oxidation behaviour of the alloy, and no evidence has been obtained in this study to disagree with this finding.

6.5. Behaviour of NiO and Metallic Nickel in the Oxide Layer

It is apparent from the free-energy diagram (fig. 12) that nickel will oxidise in carbon dioxide provided $p_{CO}/p_{CO_2} \lesssim 0.001$. Under the flow conditions maintained during the present experiments, this must certainly have been the case in the gas stream, and so is consistent with the appearance of NiO in the oxide layer formed on Inconel. The standard free-energies refer to a metal at unit activity. The activity of nickel in these alloys is less than unity and is determined to a large extent by the nickel content of the alloy, which is greater for Inconel (76 wt %) than Hastelloy (48 wt %). This can explain the formation of NiO on Inconel but not on Hastelloy.

The classical treatment of the oxidation of Ni-Cr alloys in oxygen [10] can be extended to account for the disappearance of NiO with increasing exposure time, together with the incidence of internal oxidation in the alloys. The theory states that, when the alloy is exposed, NiO and Cr_2O_3 both form initially, but rapidly combine and coalesce to give $NiCr_2O_4$ granules in a matrix of excess NiO, so effectively forming an inner layer. Partial dissociation of NiO occurs at the alloy/oxide interface and oxygen diffuses into the alloy, resulting in preferential oxidation of chromium to form Cr_2O_3 in a matrix of essentially pure nickel. Dissociation of NiO at the alloy/oxide interface may also account for the formation of voids, which may eventually contribute to loss of adhesion of the surface oxide. In the present systems, the NiO present in the initially formed surface film is almost certainly dispersed in the rhombohedral Cr_2O_3 phase, and the reaction to form the Ni-Cr spinel phase subsequently goes fairly quickly to completion in the absence of further formation of NiO.

6.6. Appearance of Porous Layers in Thick Oxide Films

It is well known that holes or pores in growing surface oxides can form as a result of coalescence of vacancies in films growing by an outward metal-diffusion mechanism. This can lead in turn to an effective increase in the length of the diffusion path for the oxidising species. Ultimately, this can result in loss of adhesion at a certain, critical, oxide thickness, although this is likely to be only a contributory factor to be taken in conjunction with the mechanical properties of the film.

6.7. Mechanical Properties of the Oxides

From the observation of conditions under which oxide spalls from some specimens, a few conclusions regarding the mechanical properties of the oxides can be drawn. No significant spalling was observed from any of the oxidations carried out on Hastelloy, but a marked degree of spalling was observed from Inconel at 800° C, to a lesser extent at 900° C, and not at all at 1000° C. In some ways, this is surprising because in both cases the oxide structure was duplex, consisting of an inner, rhombohedral oxide layer and an outer, spinel layer, and the rhombohedral layers at least did not appear to have appreciably different compositions. It is possible that this difference is associated with a mechanical keying action either by lateral surface diffusion of Cr_2O_3 or by incorporation of unreacted M_6C carbide particles from the alloy into the oxide. Alternatively, as is well known, small variations in composition can have very marked effects on oxide properties, and the experimental evidence certainly does not rule out this possibility.

Acknowledgement

This paper is published by permission of the Central Electricity Generating Board.

References

1. G. W. TITUS and J. S. BRUNHOUSE, *Corrosion* **19** (1963) 339t.
2. J. H. BUDDERY and R. J. PEARCE, *CEGB Report* No. RD/B/N.472 (1965).
3. W. P. REES, B. D. BURNS, and A. J. COOK, *JISI* **162** (1949) 325.
4. J. S. BRUNHOUSE and G. W. TITUS, *Aerojet-General Nucleonics Report* No. IDO-28605 (1963).

5. W. H. J. VERNON, F. WORMWELL, and T. J. NURSE, *JISI* **150** (1944) 81p.
6. J. M. FRANCIS, *J. Appl. Chem.* **16** (1966) 264.
7. H. J. YEARIAN, H. E. BOREN, and R. E. WARR, *Corrosion* **12** (1956) 561t.
8. S. T. WLODEK, *Trans. Met. Soc. AIME* **230** (1964) 177.
9. J. RADAVICH, "High Temperature Materials", edited by R. F. Hehemann and G. M. Ault (Wiley, New York, 1959), p. 520.
10. J. MOREAU and J. BÉNARD, *Compt. rend.* **237** (1953) 1417.